Journal of Power Sources 185 (2008) 1001–1008

Contents lists available at ScienceDirect

Journal of Power Sources

journal homepage: www.elsevier.com/locate/jpowsour

Effect of aluminizing of Cr-containing ferritic alloys on the seal strength of a novel high-temperature solid oxide fuel cell sealing glass

Yeong-Shyung Chou*, Jeffry W. Stevenson, Prabhakar Singh

K2-44, Energy Materials Department, Pacific Northwest National Laboratory, P.O. Box 999, Richland, WA 99354, United States

ARTICLE INFO

Article history:
Received 15 July 2008
Received in revised form 29 August 2008
Accepted 1 September 2008
Available online 7 September 2008

Keywords:
Seal strength
Sealing glass
Interface
Aluminization
SOFC

ABSTRACT

A novel high-temperature alkaline earth silicate sealing glass was developed for solid oxide fuel cell (SOFC) applications. The glass was used to join two metallic coupons of Cr-containing ferritic stainless steel for seal strength evaluation. In previous work, $SrCrO_4$ was found to form along the glass/steel interface, which led to severe strength degradation. In the present study, aluminization of the steel surface was investigated as a remedy to minimize or prevent the strontium chromate formation. Three different processes for aluminization were evaluated with Crofer22APU stainless steel: pack cementation, vapor-phase deposition, and aerosol spraying. It was found that pack cementation resulted in a rough surface with occasional cracks in the Al-diffused region. Vapor-phase deposition yielded a smoother surface, but the resulting high Al content increased the coefficient of thermal expansion (CTE), resulting in the failure of joined coupons. Aerosol spraying of an Al-containing salt resulted in the formation of a thin aluminum oxide layer without any surface damage. The room temperature seal strength was evaluated in the as-fired state and in environmentally aged conditions. In contrast to earlier results with uncoated Crofer22APU, the aluminized samples showed no strength degradation even for samples aged in air. Interfacial and chemical compatibility was also investigated. The results showed aluminization to be a viable candidate approach to minimize undesirable chromate formation between alkaline earth silicate sealing glass and Cr-containing interconnect alloys for SOFC applications.

1. Introduction

Among the challenges facing developers of planar solid oxide fuel cells (SOFCs) technology, a reliable and robust sealing material or system remains a high priority in research and development activities [1,2]. The sealing material or system has to be hermetic or of low leakage, electrically insulting, chemically compatible with mating materials, thermally stable, and mechanically strong in the harsh dual environment (oxidizing, wet, and reducing atmospheres) to survive numerous thermal cycles as well as long-term (~40,000 h) operation at elevated temperatures (~700–850 °C). Current SOFC seal research can be classified into three areas: glass seal [3–11], active braze [12–15], and compressive seal [16–18]. The advantages and disadvantages of these approaches have been reviewed in the literature [19,20]. Among these approaches, glass and glass–ceramics have been extensively studied due to the wide range of properties available through modification of the composition. Alkaline earth silicate glasses are among the most studied glass systems. For example, Chou et al. studied a Sr–Ca–Y–B–Si glass system with a focus on obtaining high sealing temperatures (>950 °C) for better long-term thermal and chemical stability by varying the B_2O_3 content [3]. Meinhardt et al. developed a Ba–Ca–Al–B–Si glass with a lower sealing temperature (<830 °C) [4]. Lahl et al. examined the crystallization kinetics of A–Al–B–Si glasses (A = Ba, Ca, and Mg) and the influence of nucleating agents on the activation energy of crystal growth [5]. Sohn et al. investigated the thermal and chemical stability of the Ba–Al–La–B–Si system. They found that the CTE increased with BaO content and a maximum CTE of $\sim 11 \times 10^{-6}\,^{\circ}C^{-1}$ was obtained at BaO = 40% and $B_2O_3/SiO_2 = 0.7$ [6]. Ley et al. studied the system of Sr–Al–La–B–Si glass with varying CTE in the range of $(8–13) \times 10^{-6}\,^{\circ}C^{-1}$ [7]. Adding ceramic fibers to improve the thermal cycle stability was demonstrated by Taniguchi et al. [8]. However, the complex seal system required very high compressive stress (2 kgf cm^{-2}).

In addition to close CTE match, chemical compatibility with mating SOFC components is also required for sealing glasses. As the operation temperature for SOFC has dropped from ~1000 °C to below ~800 °C, the use of Cr-containing ferritic stainless steel such

* Corresponding author. Tel.: +1 509 3752527; fax: +1 509 3752186.
E-mail address: yeong-shyung.chou@pnl.gov (Y.-S. Chou).

0378-7753/$ – see front matter © 2008 Elsevier B.V. All rights reserved.
doi:10.1016/j.jpowsour.2008.09.004

as Crofer22APU as the interconnect material appears to be feasible. However, glass/metal interaction has created another level of hurdles. The behavior of various glass–ceramics with ferritic stainless steels under SOFC environments has been investigated [9–11]. The results of as-sealed or short-term aged (<400 h) samples showed undesirable chromate formation [3,11], microstructure degradation, and electrical shorting [9]. In our earlier study of the seal strength of alkaline earth silicate sealing glass with Crofer22APU, Sr–chromate was readily formed along the glass/metal interface when exposed to air, and the seal strength almost dropped to zero after ageing in air for a few hundred hours. No strength degradation was observed when sealed coupons were aged in a reducing environment, due to fact that the chromate phase is not stable in reducing atmospheres and therefore did not form. [21]. A possible solution to the air-side chromate formation was proposed which involved aluminizing the metallic interconnect to form a protective layer of alumina. Aluminide coatings on alloys or steels are commonly applied to minimize the oxidation or increase the creep resistance of base metals. For example, pack cementation was applied with different activators on alloy steels containing 9–12 wt.% Cr and 1 wt.% Mo at 650 °C to improve its oxidation and creep resistance [22]. Houngniou et al. showed the iron–aluminide coating exhibited excellent resistance to cyclic oxidation at 1000 °C [23]. The coating was also applied to porous Ni anodes for molten carbonate fuel cells to improve the creep resistance [24] as well as in multi-component coatings of $(Fe,Cr)_3Al$ which showed no attack when tested in a simulated boiler atmosphere at 500 °C for 500 h [25]. The objective of the present study was to investigate several aluminization processes – pack cementation, vapor-phase deposition, and aerosol spraying – to form a protective alumina surface layer instead of the aluminide, and to evaluate its effect on the seal strength of a novel high-temperature sealing glass with Crofer 22APU steel. In addition, environmental effects during aging were studied. Fracture surface and microstructure analysis were conducted and correlated with results of strength testing.

2. Experimental

2.1. Sealing glass preparation

The sealing glass used in this study is a high-temperature $(SrO,CaO)–Y_2O_3–B_2O_3–SiO_2$ glass (with a mole ratio of 48.5:6:8.5:37), designated YSO75, which was prepared by conventional oxide or carbonate mixing followed by glass melting at 1500 °C for 0.5 h in a Pt-crucible. The details of glass making and heat-treatment are given in [3]. This glass was developed for higher (>950 °C) sealing temperatures than the conventional G18 (Ba–Ca–Al–B–Si) glass of sealing temperatures <850 °C [4]. The as-prepared bulk glass has a glass transition point (T_g) of 685 °C, a softening point (T_s) of 741 °C, and an average coefficient of thermal expansion (CTE) of $11.6 \times 10^{-6}\,°C^{-1}$. Partially devitrified (short-term crystallized) glass shows no distinct glass transition point, but still contains some residual glassy phase and exhibits softening at 914 °C, and a slightly higher average CTE of $11.9 \times 10^{-6}\,°C^{-1}$ [3].

2.2. Aluminization of Crofer22APU

The ferritic stainless steel Crofer22APU was chosen for the aluminization evaluation. Crofer22APU is a special ferritic stainless steel developed for SOFC applications which contains about 22 wt.% of Cr to improve the oxidation resistance while maintaining good oxide scale electrical conductivity. It also contains small amounts of impurities or additives of Mn, Al, Ti, Si, and La (<0.5–0.8 wt.%) [21,26]. The as-received Crofer22APU sheet had a thickness of 0.5 or 1.0 mm and was cut into 12.5 mm × 12.5 mm squares for coating and strength testing. Before coating, the metal coupons were ultrasonically cleaned in *iso*-propanol followed by cleaning in acetone. For aluminization via a pack cementation process, the metal coupons were embedded in a powder mixture of Al, Al_2O_3, and activator using a commercial process (NC101, Hitemco, Old Bethpage, NY). Before coating, the samples were degreased and lightly sand blasted using fine alumina powders to remove surface oxides. The samples were then processed at ~900–1100 °C for several hours in an inert atmosphere (H_2/Ar) to produce a coating thickness of ~50–100 μm. The second aluminization process was conducted via vapor-phase deposition using the same pack of powers; in this case, the metal coupons were not embedded within the powder mixture but suspended above it (VPA GP-275, Hitemco, Old Bethpage, NY). The samples were heat-treated the same as the pack cementation process. The as-prepared aluminized coupons from the pack cementation or vapor-phase process were further heat-treated in air at 1000 °C or 1200 °C for 2 h to convert the aluminide to aluminum oxide. A third process was also tested which involved air-spraying of an Al–halide in an solvent (A aerosol, ZYP Coatings, Oak Ridge, TN) a few times onto both sides of the metal coupons. After drying, the coupons were first heat-treated at 650 °C in a reducing environment for 12 h (2.7% H_2/balance He) to convert the deposited Al–halide to Al and promote the diffusion into the metal substrate. The coupons were then fired to 1000 °C for 1 h in air to form the alumina layer.

2.3. Coupon sealing, mechanical testing, and microstructure characterization

The as-prepared glass was crushed, passed through a #100-mesh sieve, and mixed with organic binders to form a paste. For coupon sealing, the paste was sandwiched between two metal coupons and dried in an oven. After drying, the couple was slowly fired to 550 °C for 2 h, then to 950–975 °C for 2 h followed by 800 °C for 4 h. To evaluate environmental aging effects, the as-sealed coupons were aged in air or in wet (~30% H_2O) dilute hydrogen (~5.2% H_2/He) at 850 °C for 300 h. For room temperature seal strength tests, the as-sealed or aged coupons were glued to two aluminum test fixtures and tested in uniaxial tension. The details of the assembly and test conditions are given in an earlier paper [21]. For each condition, about 6–7 samples were tested and the average strength was reported. After the test, fracture surfaces were examined with optical microscopy. Some of the sealed samples as well as unsealed aluminized coupons were also sectioned and polished for interfacial characterization using scanning electron microscopy (JOEL SEM model 5900LV). All the images were taken under back scattering mode.

2.4. Chemical compatibility study

To investigate the chemical compatibility of the sealing glass with alumina, the as-prepared YSO75 glass powders (~100 mesh) were mixed with alpha-alumina powder (Alfa Aesar, MA, 99.98% purity, surface area = 6 $m^2\,g^{-1}$) in a mass ratio of 2:1 in *iso*-propanol for 15 min. The slurry was then dried and sieved through a #100-mesh sieve. The mixed powders were die-pressed at 50 MPa and sintered at 950 °C for 2 h followed by heat-treatment at 800 °C for 4 h before cooling to room temperature. The ramp rate for heating and cooling was 5 °C min^{-1}. Since the sealing glass partially devitrifies readily at SOFC operating temperatures, a parallel test to understand the reaction of devitrified glass with alumina was also conducted using pre-devitrified glass powders (glass powder heat-treated at 950 °C for 2 h and 800 °C for 4 h, followed by vibration milling in a WC container and sieving through a #100-mesh

sieve). The short-term crystallized powders were then processed in the same manner as the as-prepared glass powders with alumina powders for chemical compatibility tests. After sintering, the pellets were crushed and pass through a #325-mesh sieve for X-ray diffraction analysis (Phillips XRG3000) at 40 kV and 45 mA.

3. Results and discussion

3.1. Surface morphology and cross-section of aluminized Crofer22APU

3.1.1. Pack cementation

The as-received Crofer22APU steel was rather smooth (surface roughness about 1–2 μm) since it was fabricated by rolling metal sheets down to 0.5 mm or 1 mm thickness. After pack cementation-based aluminization, the surface appeared to be much rougher (10–20 μm) and somewhat damaged as shown in the cross-section view in Fig. 1A and B. The Al-diffused region was also evident, extending from the surface to a depth of about 100 μm as shown in Fig. 1A by the different color contrast. It is worth noting that the presence of Al as aluminide in the diffused region also induced large residual tensile stresses upon cooling which caused localized cracking within the diffused aluminide layer. This is likely due to the high CTE and the brittle nature of these intermetallic aluminides. Various aluminides were reported by the pack cementation processes such as Fe_2Al_5 when using activator of AlF_3 on P92 steel (Fe–9Cr–1.0Mn–0.1C) at 650 °C [22], or Fe_3Al and FeAl when using NH_4Cl activator on Fe–30Cr at 1000 °C [23]. From EDS analysis, the chemical composition of the as-coated surface was found to have a mole ratio of (Fe,Cr) to Al = 73:27, close to 3:1 corresponding to $(Fe,Cr)_3Al$. However, the chemical compositions at a depth of 10–20 μm from the outer surface were found to have an atomic ratio of Fe:Cr:Al = 44:12:44. Whether this corresponds to a mixture of Fe–Al and Cr or solid solution of Fe–Cr–Al is not clear. Nonetheless the aluminides are known to have very large CTEs. For example, the average CTE of oxide dispersion strengthened Fe_3Al was reported to be greater than $(21–22) \times 10^{-6}\,°C^{-1}$ and $(18–21) \times 10^{-6}\,°C^{-1}$ for FeAl at temperature range 500–1000 °C [27]. The CTE of the base metal Crofer22APU is about $12.5 \times 10^{-6}\,°C^{-1}$. As a result of the large CTE mismatch between the Al-diffused region and the base metal, high residual tensile stresses developed during cooling, resulting in the observed cracking (Fig. 1B). The as-coated surface is shown in Fig. 1C with the majority of the surface being covered by the metallic coating (white phase), and some residual alumina particles from the pack formulation (dark particles).

The coated samples were further heat-treated in air at 1000 °C or 1200 °C for 2 h to form an Al_2O_3 surface layer for glass sealing. Fig. 2 shows the cross-section and the surface morphology of a sample oxidized at 1000 °C. It will be noted that the surface appears to be even rougher, with a depth close to 40–50 μm (Fig. 2A). The oxidized surface did not show a uniform dense layer (dark phase) but instead exhibited a thickness varying from ~1 μm to ~5 μm (Fig. 2B). The surface morphology consisted of a fine-featured oxidized layer with small primary particles (Fig. 2C). Spot EDS chemical analyses were also conducted on the oxidized layer as well as the base metal. The results showed that the oxidized outer layer was mainly Al_2O_3 with trace amounts of Cr and Fe, while the base metal at a location ~10 μm from the oxide layer showed a chemical composition of Fe:Cr:Al = 63:16:21, indicating that the oxidation treatment did not deplete all the bulk-diffused Al, which was about 44 at% at a similar location before the oxidation treatment. Plain Crofer22APU oxidized under the same conditions (1000 °C for 2 h) formed a dense Cr_2O_3 sub-layer about 1–2 μm thick (Fig. 3A) and an outer layer of spinel $(Mn,Cr)_3O_4$, often in the form of fine crystals (Fig. 3B). Comparing the surface morphology and cross-section chemical analysis, it was evident that the pack aluminization process is effective in suppressing the formation of a Cr-based scale, and hence is likely to help mitigate Cr volatility as well as the above-mentioned chromate formation which can result from glass/alloy interactions.

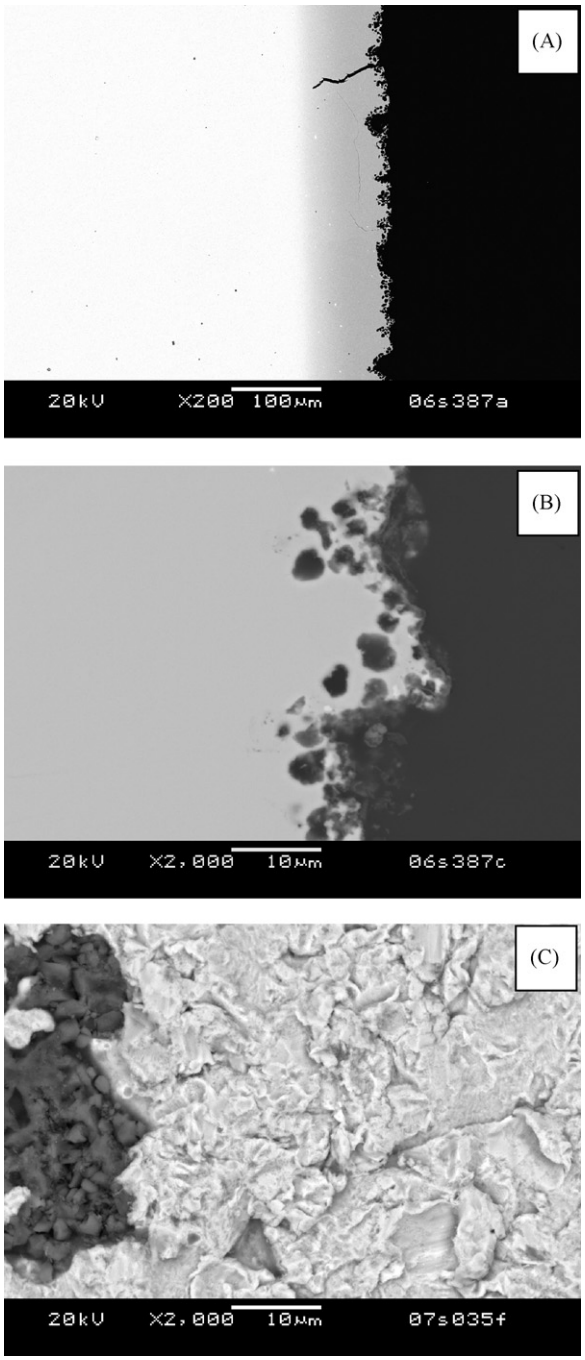

Fig. 1. SEM micrographs of as-received aluminized Crofer22APU sample made by pack cementation process. (A) A low magnification view showing the Al-diffused region and a surface crack, (B) a high magnification view near the surface, and (C) top view (dark grains were residual adhered alumina powders from pack formulation).

3.1.2. Vapor-phase deposition

A second process technique involving suspending the Crofer22APU coupons above the pack formulation was also evaluated. The objective was to minimize surface roughness as well as to pre-

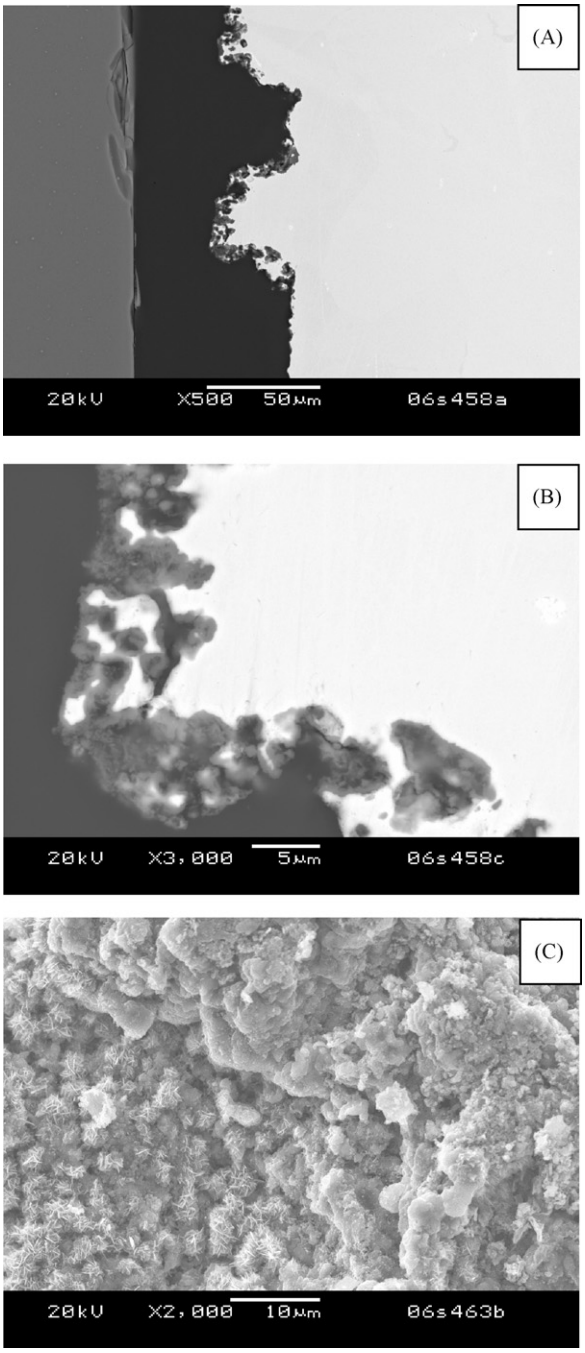

Fig. 2. SEM micrographs of aluminized Crofer22APU sample made by pack cementation process after oxidation at 1000 °C for 2 h. (A) A low magnification cross-section view, (B) a higher magnification, and (C) a top surface view.

vent the adhesion of Al_2O_3 particles which occurred in the pack cementation approach. From a sealing point of view, a slightly rough surface would be beneficial in terms of providing mechanical interlocking to improve the mechanical strength, assuming a relatively weak interface. However, surface roughness with a depth of 50 μm (as shown in Fig. 2A) or greater may present problems in terms of glass "filling" during the sealing process, resulting in residual air pockets at the interface. Fig. 4 shows cross-sections (A, B) and top surface view (C) of a vapor-phase-deposited aluminized sample after oxidation at 1000 °C 2 h. The surface was indeed much smoother as compared to the pack cementation process (Fig. 2A), with a roughness depth less than 10 μm. The alumina layer (Fig. 4B)

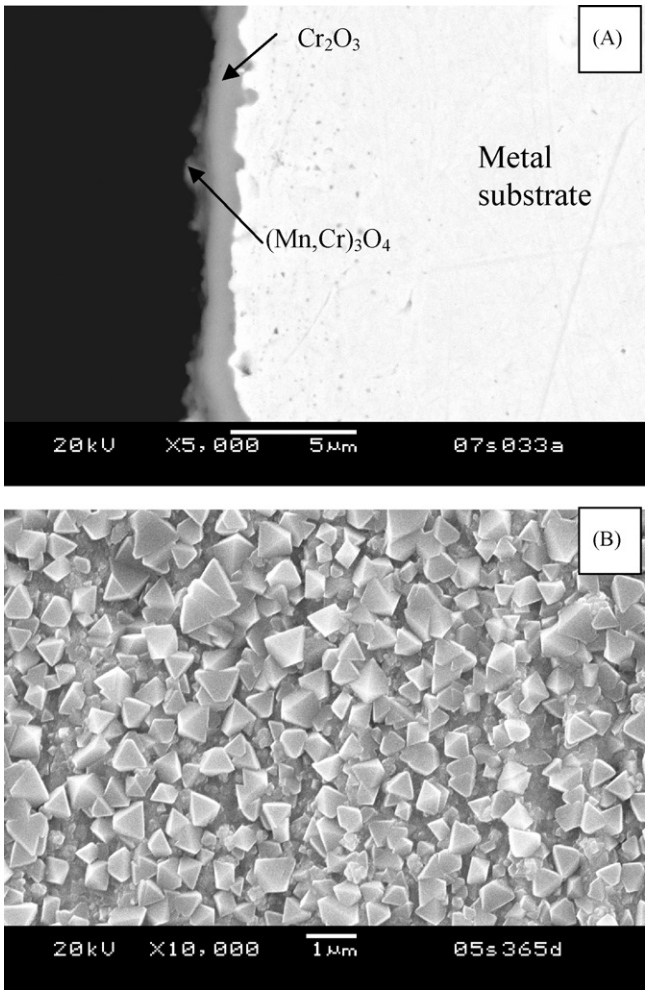

Fig. 3. (A) Cross-section and (B) top surface SEM views of plain Crofer22APU after oxidation at 1000 °C 2 h in air shows the continuous, dense Cr_2O_3 layer and a top layer of fine $(Mn,Cr)_3O_4$ crystals.

appeared to be thinner compared to the pack cementation sample (Fig. 2B). The oxidized surface showed typical alumina aggregates with small platelet-like crystals. Note that there was no clear color contrast to show the Al-diffused regions (as in Fig. 1A, which shows a gray region near the surface), and no cracks were observed. However, there appeared to be voids of the size about 10 μm beneath the surface. The formation of these voids was not clear and was expected to have minimal impact on mechanical strength since they were subsurface defects.

Attempts to create sandwich samples with these coupons were unsuccessful. Most of the coupons were completely debonded after cooling to room temperature after the high-temperature sealing/joining process. A simple linear thermal expansion test was conducted on these samples; the results are plotted in Fig. 5 together with the plain Crofer22APU base metal. It is evident that the aluminized samples exhibited a much higher CTE than the plain alloy. An average CTE of $\sim 16 \times 10^{-6}\,^{\circ}C^{-1}$ was estimated for the aluminized sample, while the plain one had a CTE of $\sim 12.5 \times 10^{-6}\,^{\circ}C^{-1}$. This large CTE mismatch and a relatively smooth surface (i.e., lack of roughness for mechanical interlocking) resulted in the fracture of the sealed coupons (recall that the CTE of the sealing glass was only $11.9 \times 10^{-6}\,^{\circ}C^{-1}$). EDS elemental analysis showed that a substantial amount of Al diffused into the thin (1.0 mm) metal substrate to a total depth of ~0.66 mm (~0.33 mm from each side). As a result of the high Al content, the CTE was much higher than the base metal.

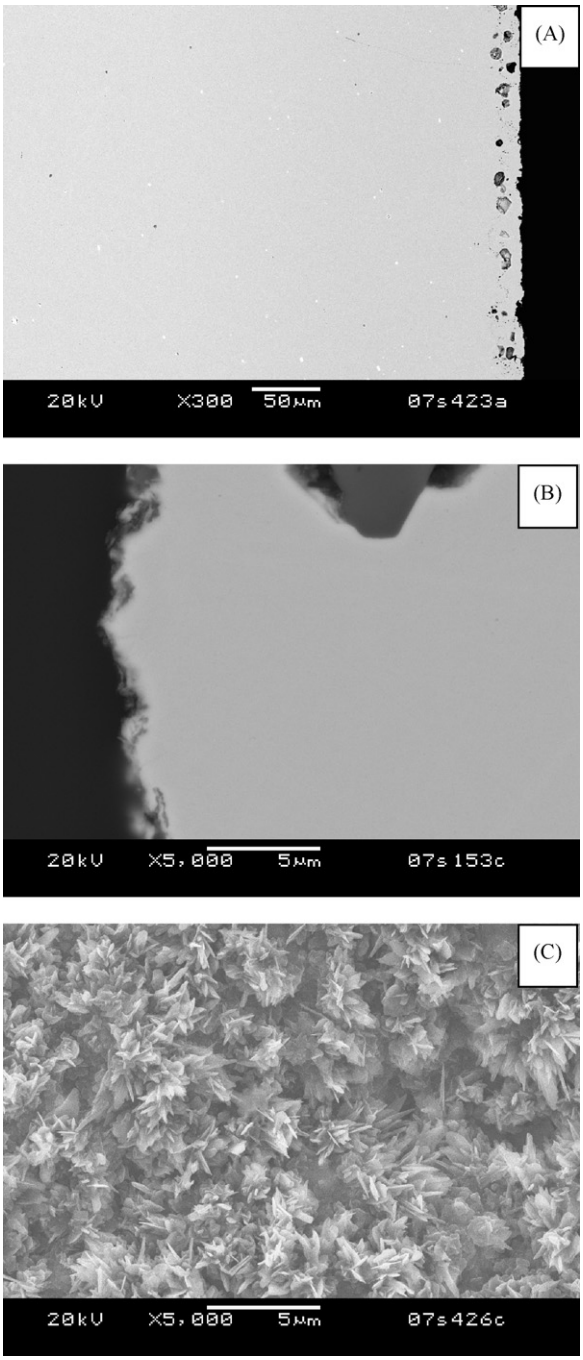

Fig. 4. (A) and (B) Cross-section and (C) top surface view of vapor-phase-deposited aluminized Crofer22APU after oxidation at 1000 °C for 2 h in air shows the much less rough surface and the fine alumina crystallites on the surface.

3.1.3. Aerosol spraying

In order to avoid substantial Al diffusion into the base metal, a third process involving simple spraying of an aerosol containing Al salts in a solvent was also evaluated. The samples were sprayed twice in an orthogonal pattern. After coating, the samples were first heat-treated in a reducing environment (650 °C for 12 h) to promote Al diffusion into the metal substrate, followed by oxidation in air. Fig. 5 shows the cross-section of an oxidized sample after the coating process. It is clear that the coating process did not lead to substantial inward Al diffusion, as most of the sprayed material remained on the surface and formed fine Al_2O_3 particles after oxidation. The minimal Al diffusion into the bulk may be due

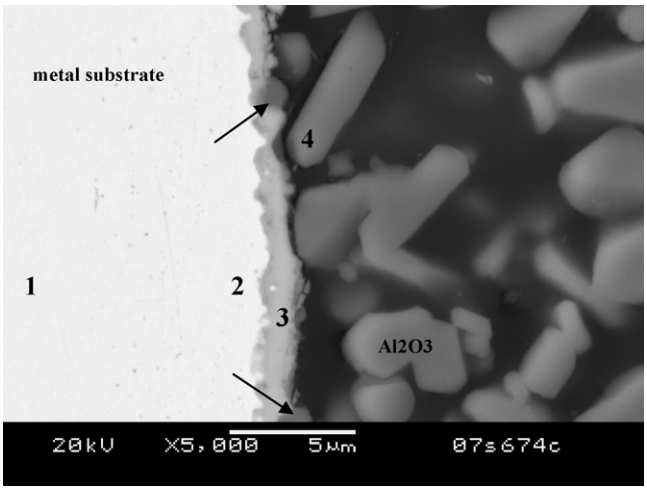

Fig. 5. Cross-section view of the aerosol sprayed Crofer22APU after oxidation. Note that many residual Al_2O_3 particles still adhered to the surface. Arrows show some fine Al_2O_3 particles on the surface layer. Chemical analysis by EDS of points 1–4 is listed in Table 1.

to a limited amount of Al available for diffusion as well as limited contact at the surface, since the aerosol spraying process resulted in a coating of very loose whitish powder. EDS analysis of the cross-section (points 1–4 in Fig. 5, also see Table 1) confirmed that most of the Al was present as relatively large discrete alumina particles above the surface scale which was composed primarily of Cr_2O_3 with trace amounts of Fe and Mn. There also appeared to be some discrete sub-μm alumina particles formed within the Cr_2O_3 layer or on top of the chromia layer (arrows in Fig. 5). Just a few μm into the bulk alloy away from the surface, no detectible Al was present. Overall, the surface was smooth without any cracks or deep cavities. This batch of samples was used for studying the effects of environmental ageing on seal strength. No spallation or debonding was observed for these samples after sealing in a sandwiched couple, which is consistent with the EDS analysis indication that there was minimal Al inward diffusion. The lack of significant Al diffusion into the alloy left the CTE of the alloy unchanged, so that it remained well-matched to that of the glass sealing material (Fig. 6).

3.2. Room temperature seal strength of pre-oxidized aluminized samples

Room temperature seal strength of the joined metal/glass/metal couples is shown in Fig. 7 for the aluminized Crofer22APU samples prepared by pack cementation. For comparison, published strength data for couples prepared with plain Crofer22APU is also included [21]. The seal strength of plain Crofer22APU, aluminized Crofer22APU pre-oxidized at 1000 °C for 2 h, and aluminized Crofer22APU pre-oxidized at 1200 °C for 2 h was 6.3 ± 0.9 MPa, 6.3 ± 2.0 MPa, and 5.1 ± 2.7 MPa, respectively. It is evident that there was little or no strength degradation for aluminized Crofer22APU as compared to plain Crofer22APU. In contrast, the seal

Table 1
Chemical analysis by EDS of selected points in Fig. 5

Element	Point 1	Point 2	Point 3	Point 4
Cr	22.7	22.4	54.1	0.8
Fe	77.3	77.6	2.5	
Al			4.6	50.6
Mn			3.6	0.5
Si				0.5
O			35.2	47.6

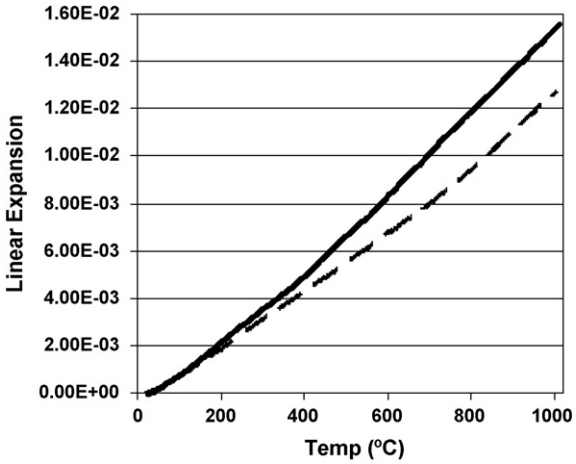

Fig. 6. Linear thermal expansion of Crofer22APU before (dotted line) and after (solid line) aluminization by the vapor-phase deposition process showing the increase of CTE from $\sim 12.5 \times 10^{-6}\,^{\circ}C^{-1}$ to $\sim 16 \times 10^{-6}\,^{\circ}C^{-1}$.

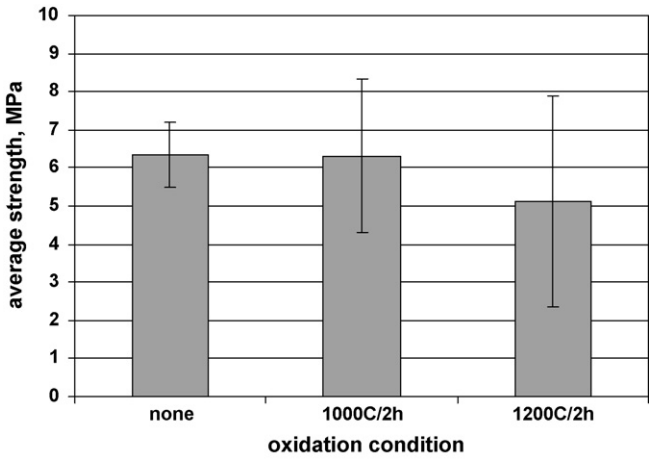

Fig. 7. Effect of oxidation of aluminized Crofer22APU coupons processed by the pack cementation process on the room temperature seal strength (seal strength data of plain Crofer22APU was from [21]).

strength of plain Crofer22APU pre-oxidized at 1000 °C 2 h was only 2.6 ± 0.8 MPa [21]. The cause for the strength degradation in the plain Crofer22APU was attributed to the formation of $SrCrO_4$ (which has very high CTE) along the metal/glass interfaces. Load and displacement curves of the aluminized samples showed typical brittle fracture with catastrophic failure at maximum load, similar to plain Crofer22APU.

3.3. Effect of environment on seal strength of aged samples

The effect of environment on seal strength of aged samples is shown in Fig. 8. For comparison, previously obtained data for plain Crofer22APU is also included. It is evident that there was no strength degradation for the aluminized samples, but instead a slight increase in strength after ageing. The as-sealed aluminized samples had a room-temperature strength of 5.8 ± 1.4 MPa, which increased after ageing in air (850 °C/300 h) to 8.2 ± 1.5 MPa, and to 8.4 ± 1.2 MPa after ageing in a wet reducing environment. On contrast, the strength of plain Crofer22APU substantially decreased to 0.5 ± 0.3 MPa after ageing in air, although it also slightly increased to 7.0 ± 1.6 MPa after ageing in wet and reducing gas [21]. It is clear that aluminization was very effective in solving the problem of strength degradation which occurred for plain Crofer22APU when aged in air. The improvement can be attributed to the presence of an outer layer of Al_2O_3 which suppressed the spontaneous formation of $SrCrO_4$ at the metal/glass interface (via reaction between oxygen in the air, Sr in the glass and Cr in the steel). From fracture surface analysis, no yellowish color (typical of $SrCrO_4$) was identified along the sealing perimeter where oxygen was available from the ambient air, suggesting that no $SrCrO_4$ formed at the interface. Similarly, no $SrCrO_4$ was found at the glass/metal interface during cross-section analysis, as shown in Fig. 9A. In contrast, the interfaces with plain Crofer22APU typically contain the chromate phase, which often cracks due to its very high, anisotropic CTE (arrows in Fig. 9B).

As noted above, aluminized samples aged in either the air or reducing environment showed some increase in strength (the standard deviation of ±1.2–1.5 MPa or 14–18% was consistent with typical brittle ceramics), although the strengths remained low compared to dense glass materials. There are several possible explanations for the observed behavior. One could be related to changes in defect morphology and/or size during the 300 h ageing. Although no direct evidence could be identified on the fracture surfaces, one may not expect to detect a decrease in critical flaw size or

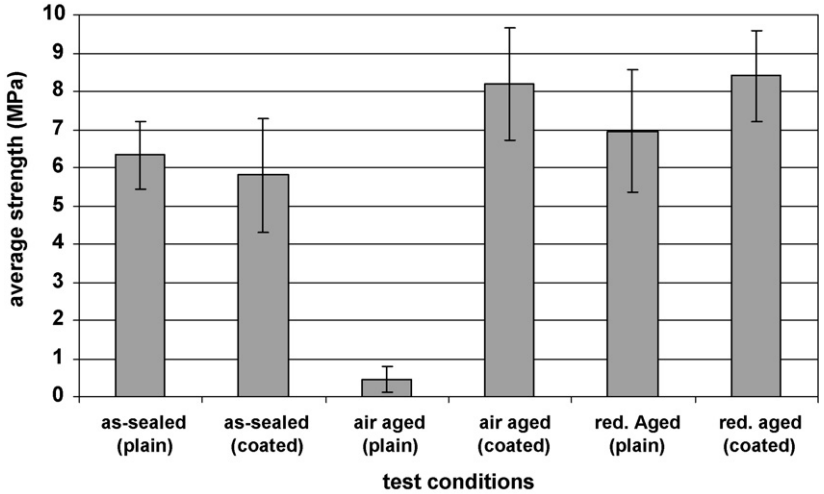

Fig. 8. Effect of environmental ageing on seal strength of aluminized Crofer22APU coupons prepared by aerosol spraying process. For comparison, seal strength of plain Crofer22APU was also included (data from [21]).

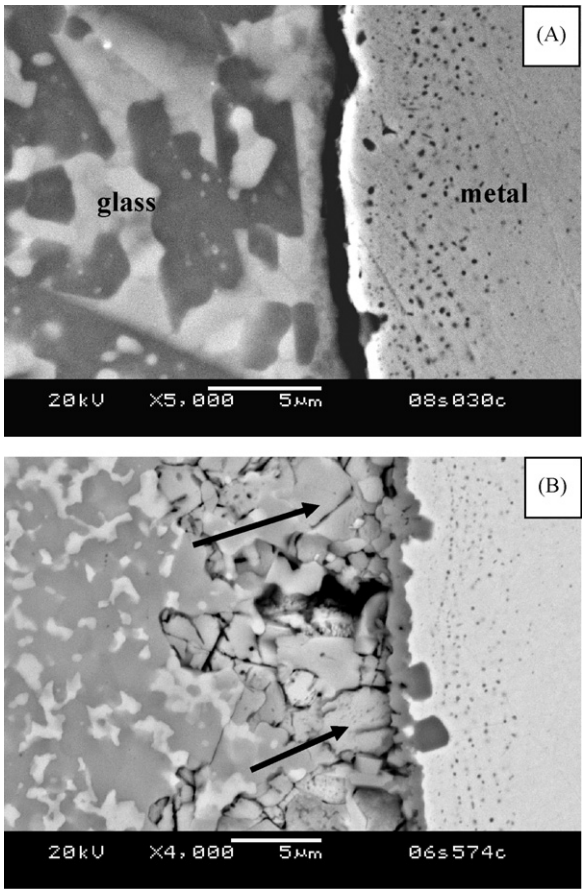

Fig. 9. Cross-section of glass/metal interface of air aged Crofer22APU, (A) aluminized sample by aerosol spraying, and (B) plain Crofer22APU (arrows are $SrCrO_4$).

morphology giving the fact the sealing glass experienced substantial viscous flow during the initial high-temperature sealing. As a result, most defects should initially have a round geometry and a smooth outer surface. As the sealing glass subsequently devitrified into a polycrystalline multi-phase mixture (with some residual glass), significant changes in the flaw size and morphology may have occurred, possibly including a reduction in the size of the critical flaws leading to failure during the tensile strength tests. The other explanation could be related to the relief of residual stresses (created as the samples were cooled from the sealing temperature of 950 °C) during the subsequent high-temperature anneal at 850 °C. The initial bulk glass, which has a CTE of $11.6 \times 10^{-6}\,°C^{-1}$ and a softening point of 741 °C, becomes more rigid after short-term crystallization, resulting in a higher softening point at 914 °C [21]. Since the metal has a higher CTE ($12.5 \times 10^{-6}\,°C^{-1}$), some residual stresses may have developed as the glass was cooled down below the softening point, which were subsequently relieved by the formation of new phases during the partial devitrification of the glass which occurred as it was aged at 850 °C for several hundred hours.

3.4. Chemical compatibility

For alkaline earth (such as Ba) silicate glasses containing aluminum, devitrification can result in formation of a stable monoclinic celsian phase ($BaAl_2Si_2O_8$), a meta-stable hexagonal celsian phase, and/or an orthorhombic (paracelsian) phase. The monocelsian is stable from room temperature to 1590 °C; above this temperature hexa-celsian is stable up to the melting point of 1760 °C [28]. The formation of the celsian phases can cause problems due to their low CTE; mono- and hexa-celsian phase have a CTE of $3.0 \times 10^{-6}\,°C^{-1}$ and $8.0 \times 10^{-6}\,°C^{-1}$, respectively. In addition, there is a dimensional change (4%) during the reversible transformation between the orthorhombic and hexagonal phase. In our earlier thermal properties study of a Ba–Ca–Al–B–Si glass, hexacelsian phase was formed initially and then gradually transformed into the more stable monoclinic phase, resulting in a decrease in bulk CTE after ageing at 750 °C for 1000 h [28]. Because Sr is very similar to Ba in terms of valence and ionic size, one may expect similar celsian phases may form if aluminum is present. The glass used in the present study did not contain aluminum, but of course the aluminized steels had alumina surface layers, so it was important to investigate the chemical compatibility between the glass and coated steel. Both the as-prepared glass powder and powders from crystallized glass were mixed with alumina powders and heat-treated. XRD patterns of the heat-treated mixtures are shown in Fig. 10, along with patterns for the glass powders. As expected, the as-prepared glass was amorphous with no distinct diffraction peaks. For the crystallized glass, the major crystalline phases were $SrSiO_3$, Ca_3SiO_5 and/or Ca_2SiO_4. It also contained minor phases of SrB_2O_4 and Y_2SiO_5. Similar $BaSiO_3$, $CaSiO_3$, and $MgSiO_3$ crystalline phases have been identified for Ba–Al–Si, Ca–Al–Si, and Mg–Al–Si sealing glasses, respectively [5]. The XRD pattern of the heat-treated mixture of as-prepared glass and alumina was very similar to the heat-treated mixture of crystallized glass and alumina. Two additional phases were identified: $Sr_2Al_2SiO_7$ and $SrAl_2Si_2O_8$. The mixture of as-prepared glass and alumina powders showed a more distinct presence of $SrAl_2Si_2O_8$ (number 8 in Fig. 10, pattern C) than that of the crystallized glass and alumina mixture (pattern D). This may suggest that the formation of $SrAl_2Si_2O_8$ from the reaction of glass and Al_2O_3 is more favorable, consistent with the fact that unordered (amorphous) phases should be more reactive (less constraint for atoms to reorganize) than ordered crystalline phases. This indicates that devitrifying glasses may have an advantage over non-crystallizing glasses for high-temperature SOFC sealing applications. $SrAl_2Si_2O_8$ is chemically analogous to celsian ($BaAl_2Si_2O_8$) phase; the thermal expansion coefficients are not known but are expected to be low. In addition, another tetragonal phase, $Sr_2Al_2SiO_7$, was found in the sintered powder mixtures, but again no published CTE data was available. Overall, the study of the powder mixtures did indicate some reaction between glass

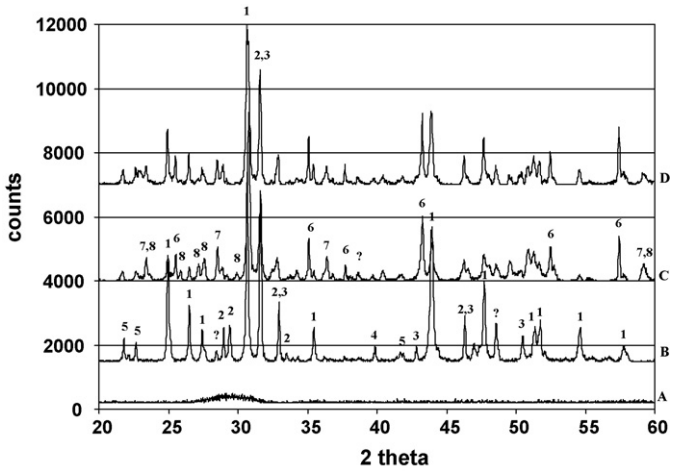

Fig. 10. XRD of the chemical compatibility study of YSO75 glass and alumina powders. (A) As-made YSO75 glass, (B) crystallized glass, (C) sintered mixture of as-made glass and alumina, and (D) sintered mixture of crystallized glass and alumina. 1: $SrSiO_3$, 2: Ca_3SiO_5, 3: Ca_2SiO_4, 4: SrB_2O_4, 5: Y_2SiO_5, 6: Al_2O_3, 7: $Sr_2Al_2SiO_7$, and 8: $SrAl_2Si_2O_8$.

YSO75 and alumina. On the other hand, no distinct crystalline phases of $SrAl_2Si_2O_8$ or $Sr_2Al_2SiO_7$ could be identified along the metal/glass interfaces of the sealed coupon samples during post-strength test analysis, suggesting that any reaction that did occur was very limited.

4. Summary and conclusion

The problem of strength degradation of SOFC sealing glass/metallic interconnect interfaces was addressed with aluminizing processes. Three different process techniques were briefly evaluated. The pack cementation process resulted in a rough surface with localized surface cracks. The vapor-phase process yielded a smoother surface morphology; however, care must be taken to minimize overdosing Al, which can lead to a significant increase in CTE. A simple aerosol spray formed a very thin and discrete alumina layer. High-temperature ageing of sealed, aluminized metal couples resulted in increased strength, in contrast to the severe strength degradation observed for non-aluminized coupons. XRD patterns indicated some potential reactivity between the sealing glass and alumina to form secondary phases; however, none of these phases could be confirmed on the sealed coupons. Overall, aluminization appears to be a viable approach to prevent adverse reaction between Cr-containing metallic interconnects and alkaline earth silicate sealing glasses.

Acknowledgements

The authors would like to thank S. Carlson for SEM sample preparation, and J. Coleman for SEM analysis. Charles Berger of Hitemco, Inc. provided experimental details regarding the pack cementation and vapor-phase aluminization processes. This work summarized in this paper was funded by the US Department of Energy's Solid-State Energy Conversion Alliance (SECA) Core Technology Program. Pacific Northwest National Laboratory is operated by Battelle Memorial Institute for the US Department of Energy under Contract No. DE-AC06-76RLO 1830.

References

[1] N.Q. Minh, J. Am. Ceram. Soc. 76 (3) (1993) 563–588.
[2] B.C.H. Steele, J. Mater. Sci. 36 (2001) 1053–1068.
[3] Y.-S. Chou, J.W. Stevenson, P. Singh, J. Electrochem. Soc. 154 (7) (2007) B644–B651.
[4] K.D. Meinhardt, D.-S. Kim, Y.-S. Chou, K.S. Weil, J. Power Sources 182 (1) (2008) 188–196.
[5] N. Lahl, K. Singh, L. Singheiser, K. Hilpert, D. Bahadur, J. Mater. Sci. 35 (2000) 3089–3096.
[6] S.-B. Sohn, S.-Y. Choi, G.-H. Kim, H.-S. Song, G.-D. Kim, J. Non-Cryst. Solids 297 (2002) 103–112.
[7] K.L. Ley, M. Krumpelt, R. Kumar, J.h. Meiser, I. Bloom, J. Mater. Res. 11 (6) (1996) 1489–1493.
[8] S. Taniguchi, M. Kadowaki, T. Yasuo, Y. Akiyama, Y. Miyake, K. Nishio, J. Power Sources 90 (2) (2000) 163–169.
[9] V.A.C. Haanappel, V. Shemet, S.M. Gross, Th. Koppitz, N.H. Menzler, M. Zahid, W.J. Quadakkers, J. Power Sources 150 (2) (2005) 86–100.
[10] N. Lahl, D. Bahadur, K. Singh, L. Singheiser, K. Hilpert, J. Electrochem. Soc. 149 (5) (2002) A607–614.
[11] Z. Yang, K.D. Meinhardt, J.W. Stevenson, J. Electrochem. Soc. 150 (8) (2003) A1095–A1101.
[12] K.S. Weil, J.S. Hardy, J.Y. Kim, J. Adv. Spec. Mater. V: Am. Soc. Met. 5 (2000) 47–55.
[13] J. Duquette, A. Petric, J. Power Sources 137 (1) (2004) 71–75.
[14] M.C. Tucker, C.P. Jacobson, L.C. De Jonghe, S.J. Visco, J. Power Sources 160 (2) (2006) 1049–1057.
[15] K.S. Weil, C.A. Coyle, J.T. Darsell, G.G. Xia, J.S. Hardy, J. Power Sources 152 (1) (2005) 97–104.
[16] S.P. Simner, J.W. Stevenson, J. Power Sources 102 (1–2) (2001) 310–316.
[17] Y.-S. Chou, J.W. Stevenson, J. Power Sources 112 (1) (2002) 130–136.
[18] Y.-S. Chou, J.W. Stevenson, J. Power Sources 125 (1) (2004) 72–78.
[19] P. Lessing, J. Mater. Sci. 42 (2007) 3465–3476.
[20] J.W. Fergus, J. Power Sources 147 (1) (2005) 46–57.
[21] Y.-S. Chou, J.W. Stevenson, P. Singh, J. Power Sources 184 (2) (2008) 238–244.
[22] Z.D. Xiang, P.K. Datta, J. Mater. Sci. 40 (2005) 1959–1966.
[23] C. Houngniou, S. Chevalier, L.J. Larpin, Oxid. Met. 65 (5–6) (2006) 409–418.
[24] H.S. Chun, G.P. Park, J.H. Lim, K. Kim, J.K. Lee, K.H. Moon, J.H. Youn, J. Power Sources 49 (2) (1994) 245–255.
[25] M. Zheng, R.A. Rpp, Oxid. Met. 49 (112) (1998) 19–28.
[26] Z.G. Yang, M.S. Walker, P. Singh, J.W. Stevenson, T. Norby, J. Electrochem. Soc. 151 (2004) B669–B681.
[27] I.G. Wright, B.A. Pint, P.F. Tortoreelli, Oxid. Met. 55 (3–4) (2001) 333–360.
[28] H.C. Lin, W.R. Foster, Am. Miner. 53 (1–2) (1968) 134–144.